Results from the Advanced Scintillator Compton Telescope (ASCOT) balloon payload

Sharma, Tejaswita
Bloser, Peter Forbes
Ryan, James M.
Legere, Jason S.
McConnell, Mark L.

To be published in:

DOI to publisher's version: 10.1117/12.2576108

Results from the Advanced Scintillator Compton Telescope (ASCOT) Balloon Payload

Tejaswita Sharma*[a], Peter F. Bloser[b], James M. Ryan[a], Jason S. Legere[a], Mark L. McConnell[a,c]
[a]Space Science Center, University of New Hampshire, Durham, NH 03824, USA; [b]Los Alamos National Laboratory, Los Alamos, NM 87545, USA; [c]Southwest Research Institute, Dept. of Earth, Oceans, and Space, Durham, NH 03824, USA

ABSTRACT

The Advanced Scintillator Compton Telescope (ASCOT) is a medium-energy gamma-ray Compton telescope flown on NASA's high-altitude scientific balloon from Palestine, TX on 5th July 2018. It uses commercially available high-performance scintillators like Cerium Bromide ($CeBr_3$) and p-terphenyl along with compact readout devices - silicon photomultipliers (SiPMs) - for an improved instrument response. ASCOT was built to address the existing need for observations in the gamma-ray energy range of 0.4 - 20 MeV. Operating stably throughout the mission, it reached an altitude of 120,000 ft and observed the Crab Nebula at MeV energies for ~5 hours. Built on the legacy of COMPTEL (onboard CGRO), along with the hardware advancement ASCOT also makes use of the Time-of-Flight (ToF) background rejection technique for effective imaging. Presented here is the Energy and ToF calibrated flight data with optimal data cuts (Earth Horizon Cut, Pulse Shape Discrimination Cut). The growth curves generated using this data from 5 to 100 g/cm^2 of residual atmosphere in conjunction with the Monte Carlo simulations of the instrument response have been used to obtain the Cosmic Diffuse Gamma-ray (CDG) flux value of $(1.28 \pm 0.37)\times10^{-5}$ photons/cm^2/s/sr/keV for 0.4 – 0.7 MeV energy range. The 3σ upper limit for CDG flux is 1.8×10^{-5} photons/cm^2/s/sr/keV for 0.7-1.5 MeV and 2×10^{-6} photons/cm^2/s/sr/keV for 1.5-2.5 MeV. The analysis of the Crab Nebula from flight observation is underway.

Keywords: Gamma Rays; Compton Telescopes; Scintillators; Silicon Photomultipliers; Balloon Instruments; Astronomy

1. INTRODUCTION

The Advanced Scintillator COmpton Telescope (ASCOT) is a medium-energy gamma-ray Compton telescope built to address the urgent need for observations in the 0.4 - 20 MeV band. ASCOT was flown on a high-altitude balloon from NASA's Columbia Scientific Balloon Facility (CSBF) in 2018 with the primary goal of observing the Crab Nebula. The analysis of the float data to image the Crab is ongoing. Here we report a new measurement of the Cosmic Diffuse Gamma-ray (CDG) background near 1 MeV using ASCOT flight data.

Observations from radio to gamma rays have all shown the presence of a diffuse background emission. Important information about various astrophysical phenomenon is carried by the isotropic CDG in the so-called medium energy gamma ray band ranging from a few hundred keV to several MeV. These gamma rays have very low interaction probability, which makes them an ideal tool to probe very early epochs of our universe.

In examining the extragalactic diffuse spectrum from the X-ray to gamma-ray region, a large number of possible origins for the diffuse gamma-ray emission have been proposed over the years. The known main components that constitute CDG extragalactic background are a combination of Seyfert I and Seyfert II Galaxies[1], Type Ia Supernovae[2] and Blazars[3]. A composite multi-wavelength energy spectrum[4] for extragalactic diffuse background is seen in Fig 1, with observations made by several missions and experiments ranging over a wide energy range.

ASCOT provides the observational data to the CDG energy spectrum in the energy range of 0.4 - 2.5 MeV, which is useful in re-establishing and updating the current model for the CDG background, as even the most recent measurements are a few decades old. COMPTEL onboard NASA's CGRO mission launched in 1991, and the Solar Maximum Mission (SMM) launched in 1980 are two of the important missions that contributed greatly in the medium energy gamma ray band[5,6].

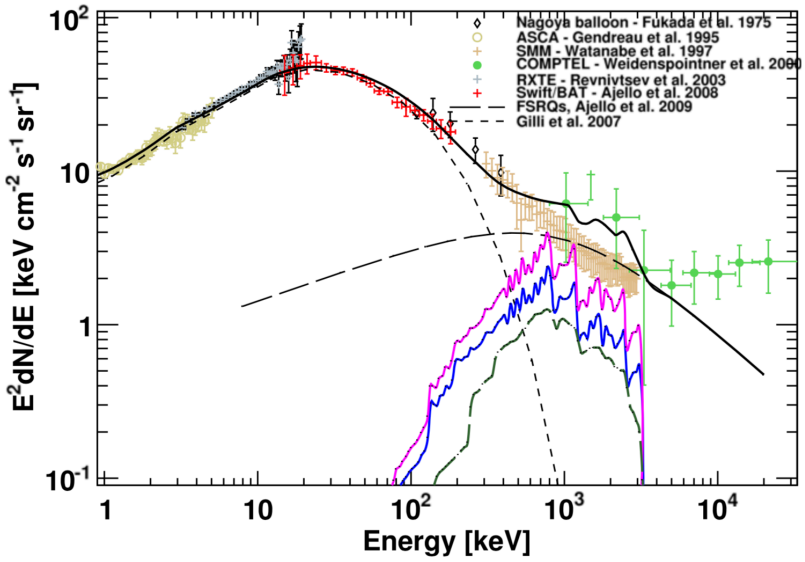

Figure 1. Cosmic gamma-ray background from different experiments and sources in the 1–30,000 keV range. The predicted contribution by SNe Ia rates from CANDELS[7] is shown in dot-dashed dark-green line, while the blue and magenta correspond to the 1σ and 2σ upper bounds on rates calculated from Subaru/XMM-Newton[8] respectively. The long-dashed black line is the contribution from flat-spectrum radio quasars[9], and the total gamma-ray background is shown by the solid black line (Figure courtesy: Ref [4]).

A major reason for such large gaps in the observational data is the fact that medium-energy gamma ray band is one of the most challenging range to observe. It is the penetrating power of MeV gamma rays that make these photons valuable as probes of energetic objects but at the same time makes them really difficult to measure. The photons in the medium energy gamma ray band interact with matter via Compton scattering and have small interaction probabilities. In an orbital environment, cosmic-ray and neutron interactions with the payload or bus produce intense backgrounds in this energy range. These large background makes for poor sensitivity and the transparency of the materials in this band makes imaging even more difficult. All these factors together add up to make this energy range one of the most difficult to observe. The issue of instrumental background in the energy range of 0.5 - 8 MeV has been a major source of error in the measurements. It has been shown[10] that cosmic ray induced radioactivity in instruments produces a large flux at around 1MeV. It is very important to separate the diffuse and induced components unambiguously for correct interpretations of data.

The problem of background was not only addressed while designing ASCOT, but suitable measures were also taken to deal with it effectively. One of the many ways to reduce background is by minimizing the passive material and using active shielding. ASCOT was surrounded by plastic anti-coincidence shields to reject charged particles. Techniques like the Pulse Shape Discrimination (PSD) are used to exclude events triggered by neutrons, and the Time of Flight (ToF) method is applied in order to reject photons coming from all other directions except for top to bottom. Thus, ASCOT flight data with better energy resolutions combined with effective background rejection techniques is promising in providing an observation set with low instrumental background compared to the Compton Telescopes flown previously and help better the current models.

2. THE ASCOT INSTRUMENT

ASCOT was designed to address the issues of the medium energy gamma ray band and is based on the legacy of NASA's COMPTEL[11]. It is a new and improved prototype[12,13] that uses advanced scintillator materials and light readout device combined with effective background rejection techniques.

2.1 Compton Telescopes

Compton telescopes are the instruments of choice for spectroscopic imaging of the sky in this difficult medium-energy gamma range. They employ two scintillator detector arrays - the Compton scattering layer (D1) made up of low Z material for high scattering probability and the absorption layer (D2) made of high Z material to absorb the scattered photon. Compton scatters in D1 are measured for location, energy deposit and pulse shape. Whereas location and energy deposit

are measured in D2 along with the time-of-flight (ToF) between D1 and D2 hits. From the positions and energy deposits in the two detectors and using the Compton scattering formula, the Compton Scatter Angle ϕ can be computed. The source of the incident gamma-ray photon could be constrained to lie on an "event circle" defined by a cone (Compton Cone) with an opening angle θ around the direction of the scattered gamma ray photon as seen in Fig 2. Events for which the pulse shape indicates a gamma-ray interaction and the ToF value corresponds to a forward-scattered photon are selected, which proves crucial to achieving a useful signal-to-noise ratio by rejecting a considerable amount of background.

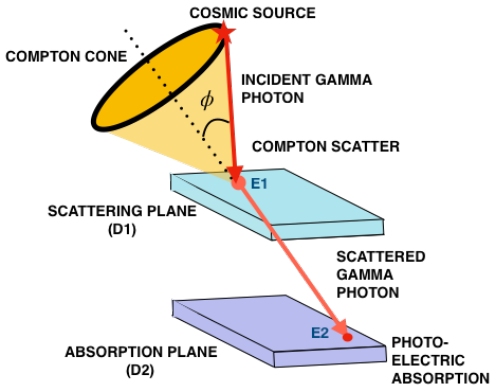

Figure 2. Schematic diagram showing the principle of a Compton Telescope. A gamma photon gets Compton scattered in D1 depositing energy E1, the scattered photon then continued on before getting absorbed in D2 depositing energy E2. Using the energies E1 and E2 the Compton Scatter Angle ϕ can be computed, which as seen here is the opening angle of the Compton cone centered at the scatter vector.

2.2 Scintillators

ASCOT uses p-terphenyl crystals (from Proteus Inc.) in the scattering detector layer (D1) with each detector element being 15×15×25 mm^3 in size. The advantages of p-terphenyl[14] over liquid scintillators include low atomic number, fast decay time, high light output and mechanical robustness. The absorption layer (D2) is made of Cerium Bromide ($CeBr_3$) which is hermetically sealed with a quartz entrance window (assembly provided by Scionix Holland/Berkeley Nucleonics Corp.). $CeBr_3$ has an edge over previously used NaI, in its high stopping power, fast timing, better energy resolution and detection efficiency. A module in each of the layers D1 & D2 consists of 64 (8x8 array) pixels as shown in Fig 3.

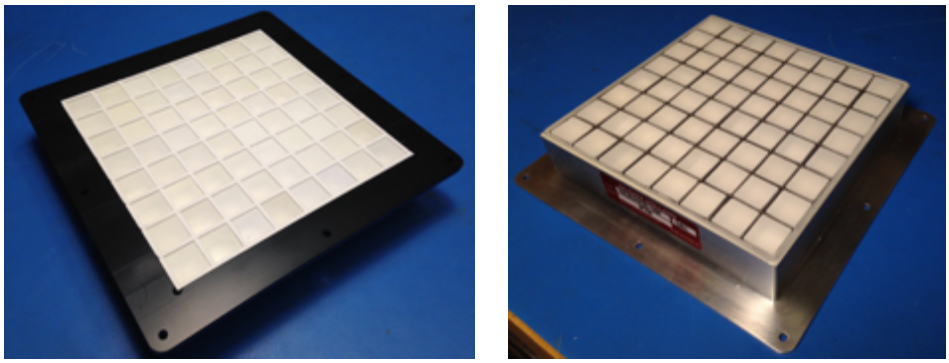

Figure 3. D1 module (Left) with 64 p-terphenyl crystals and D2 module (Right) with hermetically sealed $CeBr_3$.

2.3 Silicon Photomultiplier (SiPM)

MicroFB-60035-SMT from SensL Corp. with a Silicon Photomultipliers (SiPMs) sub-array of 2x2 is used to readout a scintillator element both in D1 & D2. SiPMs have fast response time along with high gain and when compared to Photo-multiplier Tubes (PMTs) they require lower operating voltage and are more compact and rugged. Fig 4 shows a SiPM readout board to be coupled to a D1 module.

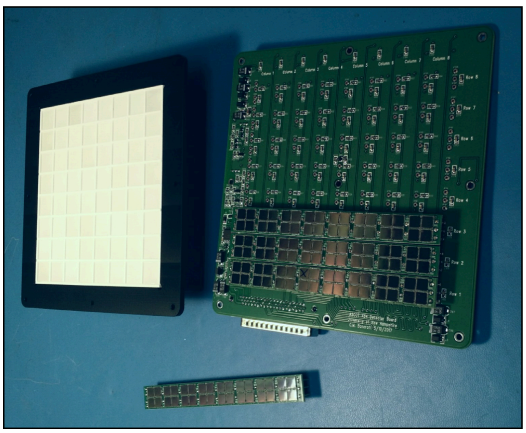

Figure 4. Seen here is a SiPM readout board populated with three SiPM strips and another on the side. This readout board will be coupled to the D1 Module shown alongside.

2.4 Instrument Assembly

The ASCOT instrument is made up of eight modules arranged in two D1 layers and four modules in the D2 layer. Each module consists of an 8x8 scintillator array coupled to a SiPM readout board. The separation between the D1 and D2 layer is determined in order to increases the efficiency and field of view of the telescope, and also to enable a good ToF resolution. The center-to-center separation between the lower D1 layer and the D2 layer is 13.25 cm. In order to minimize the locally produced background, the layers are held in place using Delrin plastic and T-slot pieces made of CPVC plastic are used for the instrument frame.

Further, in order to reject charged particle events, the modules are surrounded on all six sides by plastic anti-coincidence shields. The plastic panels are held in Delrin frames and read out by SensL SiPMs[12]. The summed SiPM signals are digitally marked in order to distinguish events produced by cosmic rays.

A small plastic scintillator infused with ~20 nCi of ^{60}Co is placed in the center of the telescope between D1 & D2 to be used as a tagged calibration source and the signals from this are read out by a SensL J-series SiPM. The tagged source enables correction to gain variations that occur during the flight in the post-flight data analysis. Fig 5 shows both the illustrated and the assembled ASCOT instrument.

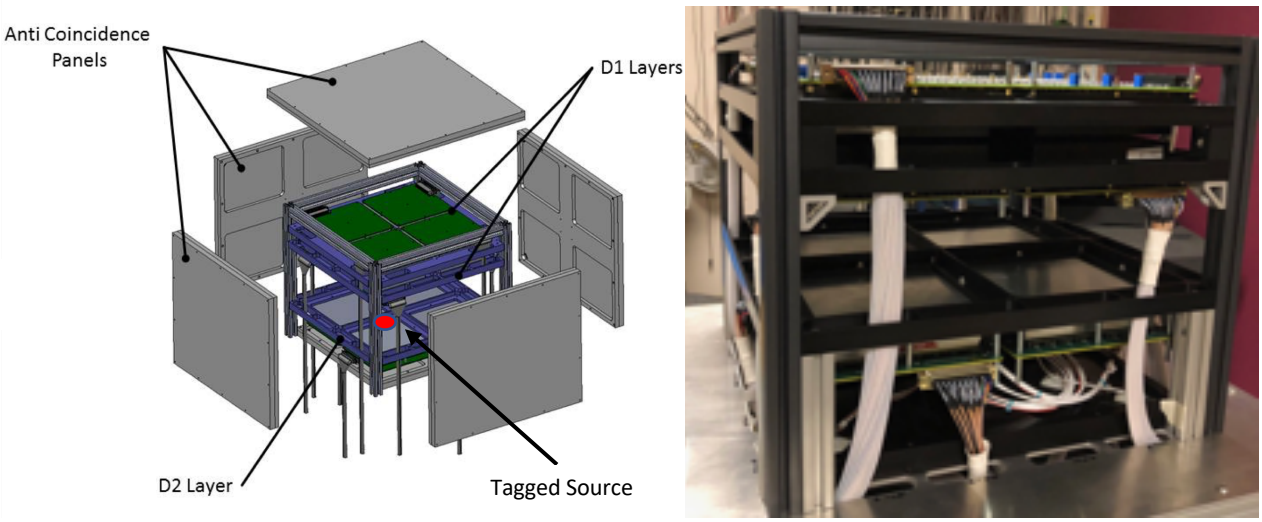

Figure 5. On the left is a schematic drawing of ASCOT showing different layer, the six anti-coincidence panels and the calibration source. The assembled instrument in the laboratory is shown on the right.

2.5 Electronics

The readout electronics is housed in an electronics box below the instrument as seen in Fig. 6. Each module is coupled to a Detector "Logic" Board which contains eight constant-fraction discriminators (CFDs) to read the fast SiPM signals from the rows and eight energy/PSD measurement channels to read the standard SiPM signals from the columns. A ToF board converts the time from the CFD trigger to a ToF value. A Module Interface Board (MIB) carrying a Xilinx FPGA controls the data acquisition as well as formats the data packets.

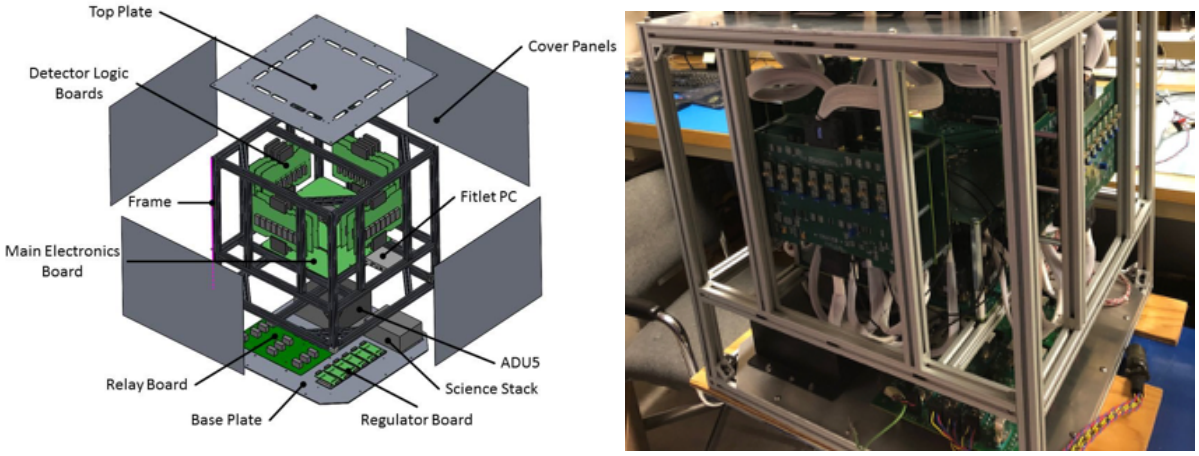

Figure 6. A schematic drawing and the assembled instrument showing the electronics box with logic boards, MIB, ToF board, Fitlet-H computer, relay board, voltage regulators, and CSBF science stack.

3. CALIBRATION

3.1 Energy Calibration

The instrument was energy-calibrated in the laboratory using various radioactive sources. 60 keV photo peak from ^{241}Am and the two Compton Edges for ^{22}Na were used to calibrate the D1 layer. 356 keV from ^{133}Ba, 511 keV and 1275 keV photo peaks from ^{22}Na along with 662 keV from ^{137}Cs, 1173 keV, 1332 keV from ^{60}Co and 2223 keV from neutron capture were used for D2 energy calibration (Fig 7).

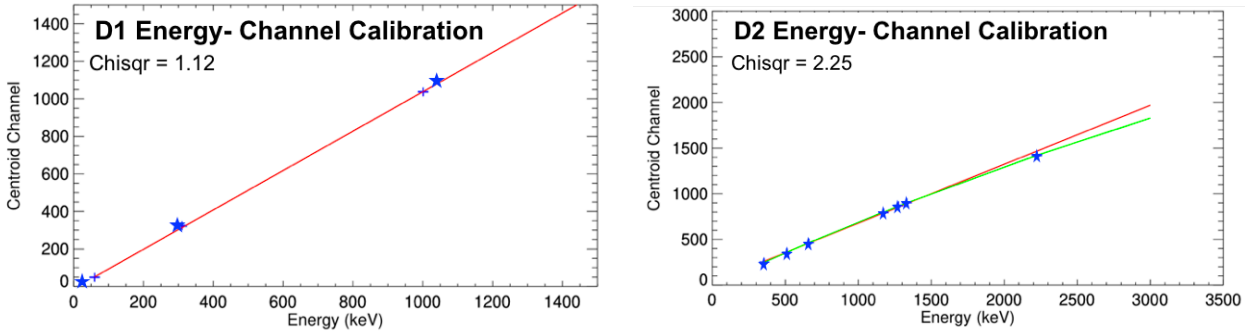

Figure 7. A schematic drawing and the assembled instrument showing the electronics box with logic boards, MIB, ToF board, Fitlet-H computer, relay board, voltage regulators, and CSBF science stack.

Since there were 512 detector channels in D1 and 256 detector channels in D2, fitting procedure was semi-automated due to these large numbers. Fig 8 shows calibrated single pixels each in D1 and D2 for which the typical energy resolution values are 30% and 6% (FWHM) respectively.

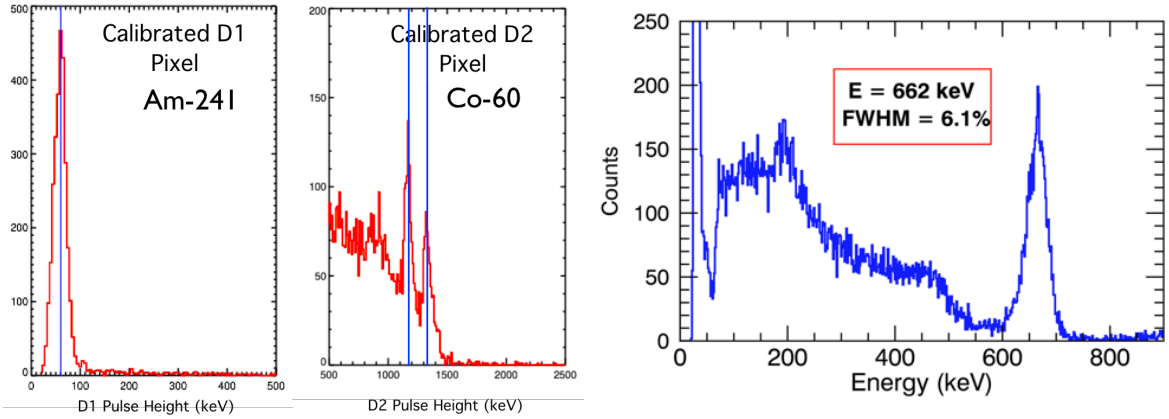

Figure 8. Energy calibrated spectra for Am-241 (60 keV) for a single pixel in a D1 module and for Co-60 (1173 keV, 1332 keV) for a single D2 pixel. The blue plot shows the calibrated energy spectrum from a single pixel from Cs-137 (662 keV) with an energy resolution of ~6%.

After calibrating all the channels, the resolution for the whole instrument (all channels combined) was determined using the spectrum obtained by placing a ^{137}Cs source above the instrument and it comes out to 9.3% at 662 keV (Fig 9). Monte Carlo simulations of the ASCOT balloon instrument were performed using the Medium Energy Gamma-ray Astronomy library (MEGAlib)[15,16], which is a set of software tools designed to simulate and analyze data of gamma-ray detectors, with a specialization on Compton telescopes. For detailed modeling of different detector types and characteristics, MEGAlib contains a geometry and detector description tool that provides an easy to use simulation program based on Geant4. A mass model of ASCOT was generated, and the instrument response was simulated for ^{137}Cs with the same position as done during the laboratory test. The resolution obtained from the simulations is 8.7% at 662 keV (Fig 9).

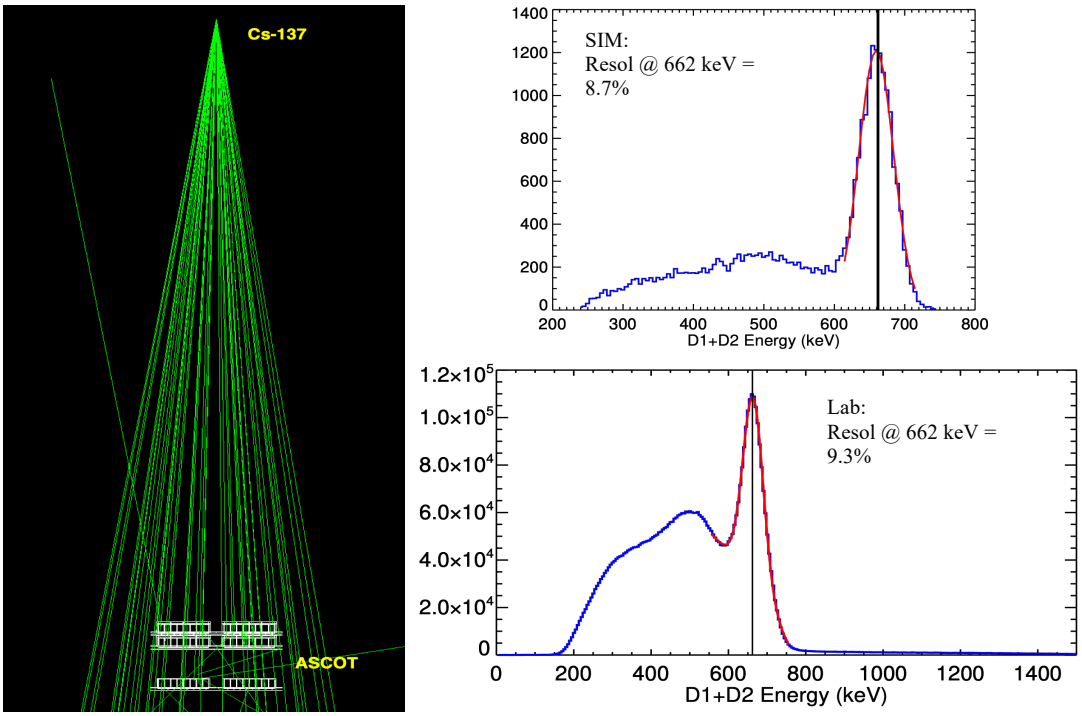

Figure 9. The instrument response was simulated for ^{137}Cs using MEGAlib and the energy resolution at 662 keV obtained thus is 8.7% whereas that obtained from the laboratory observation with a similar set-up is 9.3%.

3.2 Pulse Shape Discrimination (PSD)

The pulse-shape in the D1 pixels depend on the type of the particle being detected. This attribute lets us use the Pulse Shape discrimination as an effective background rejection technique by helping to distinguish if a detected event is from a gamma photon or a neutron. The events arising from neutrons can then be rejected to improve the instrument sensitivity. Since the shape of the voltage pulse depends somewhat on its pulse-height and may delay signals from the CFD (Constant Fraction Discriminator) which causes deviations in the PSD as a function of pulse-height referred to as "walk". Each of the 512 detector channel in D1 was corrected for this walk and calibrated for gamma photons using ^{22}Na source. Fig 10 shows the corrected and calibrated PSD distribution for all the channels combined both for ^{22}Na source and AmBe source and the neutrons are clearly distinguishable.

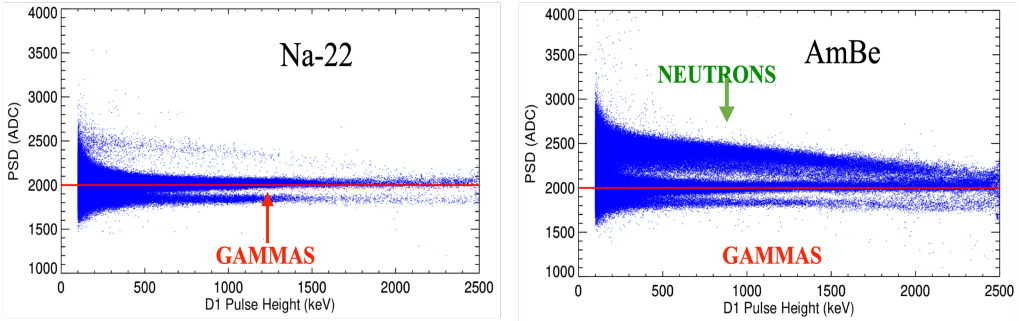

Figure 10. The above plots show calibrated and corrected PSD distribution observed in singles mode for the 512 channels of D1. ^{22}Na source which is a gamma only source was used to calibrate the PSD and the AmBe source which emits both neutrons and gammas was used to confirm that neutrons are identifiable through this method and can be rejected to improve the Signal to Noise Ratio (SNR).

3.3 Time of Flight (ToF) Calibration

Time of Flight technique is another background rejection method implemented by ASCOT in order to reject events arising from background gamma ray photons by using the timing information corresponding to the two hits in D1 & D2 layers. Since the shape of the voltage pulse generated by a signal is also dependent on the Pulse Height, this causes deviations in the ToF as a function of pulse height called 'the walk' (shown in the LEFT panels in Fig 11 & Fig 12). In order to correct this walk, ^{60}Co which is a source of coincident gamma rays (1.1 and 1.3 MeV) was placed on-axis and in between the D1 & D2 layers. This data was divided into 50keV bins and the weighted average of ToF and pulse-height for each bin was computed to determine the dependence of ToF on Pulse Height (right plot in Fig 11). The same procedure was repeated to correct the walk due to the D2 ToF circuit (Fig 12). A set of forward-scatter data using ^{60}Co source placed above the instrument was used to calibrate the 'True' ToF between any given pixel pair as shown in Fig 13.

The ToF resolution was measured for individual pixel pairs vs. energy using ^{60}Co source placed between the D1 and D2 layers. For a single pixel pair with 250 - 350 keV energy deposit in D1 and 1200 - 1400 keV energy in D2, the ToF resolution is ~480 ps (FWHM).

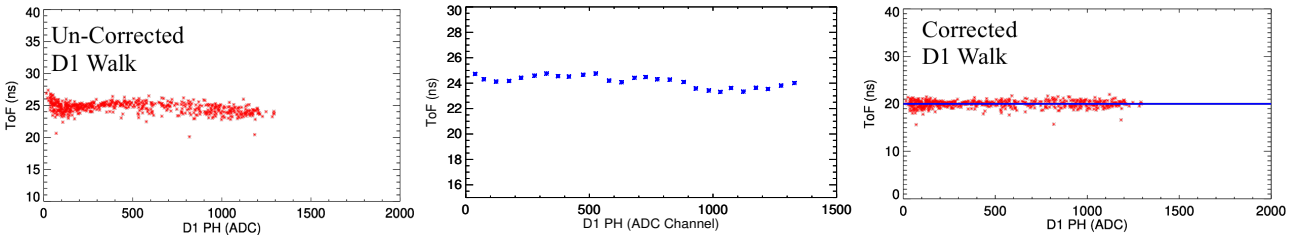

Figure 11. The Left plot shows the 'Walk' due to the D1 ToF circuit for a single pixel pair. The center plot shows the relationship between ToF and D1 pulse-height. This trend is used to correct the walk, the plot on the Right is post D1 walk correction.

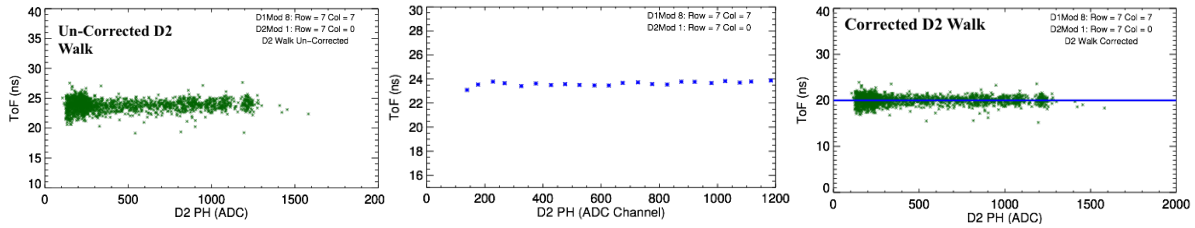

Figure 12. The Left plot shows the 'Walk' in a single pixel pair due to the D2 ToF circuit. The plot in the center shows the ToF dependence on D2 pulse-height, and the right plot shows the D2 walk corrected ToF.

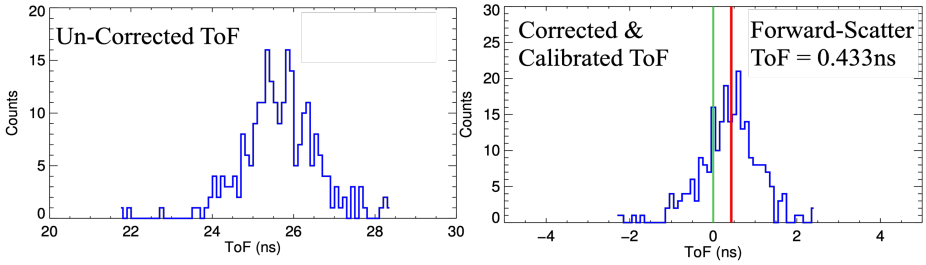

Figure 13. The ToF was calibrated by considering pixels in pairs and determining the 'True' ToF between those based on their separation. The plots here are for a pixel pair directly overhead each other with a separation of 13cm.

4. LABORATORY TESTS

The fully assembled ASCOT was used to perform the near-field source test with ^{60}Co source suspended above the instrument with the help of a crane that could be moved in x, y and z directions. The recorded events were used to generate event circles, which were then back projected onto a plane at the known source distance (in this case 'z'). Fig 14 shows the images reconstructed this way from the observed data for three different spatial source locations.

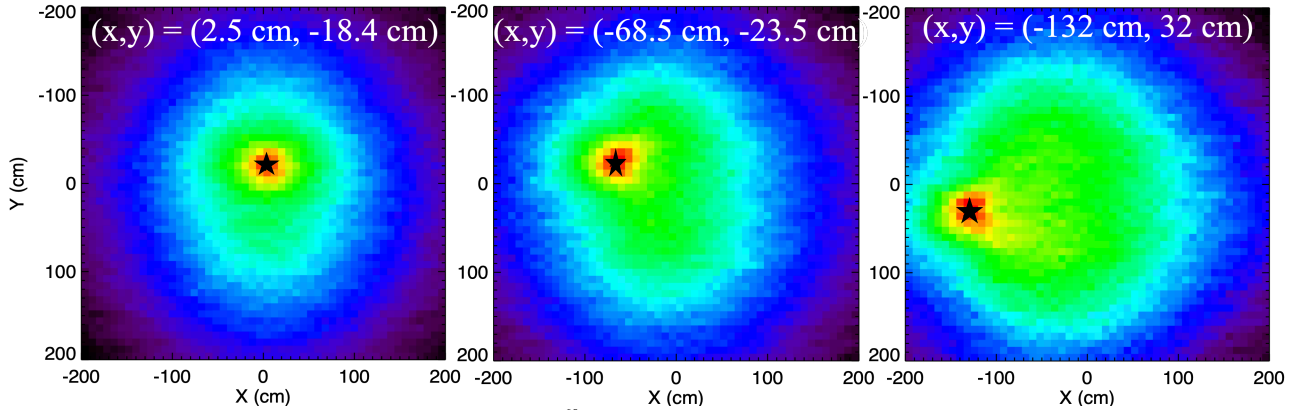

Figure 14. Image reconstruction done for a near-field ^{60}Co source by backprojecting the event circles onto a plane. The three images correspond to three different spatial locations (denoted by the black star) of ^{60}Co source.

Image reconstruction using a far-field source (Fig 15) was done with ^{252}Cf placed far above the instrument. Here the event circles were back-projected in spherical coordinates onto "the sky" instead of a plane as was done for the near-field source. Since ^{252}Cf is also a neutron emitter, this data set was used to plot PSD vs ToF which is an effective tool to visualize and distinguish the neutron events from gamma-ray events (Fig 15).

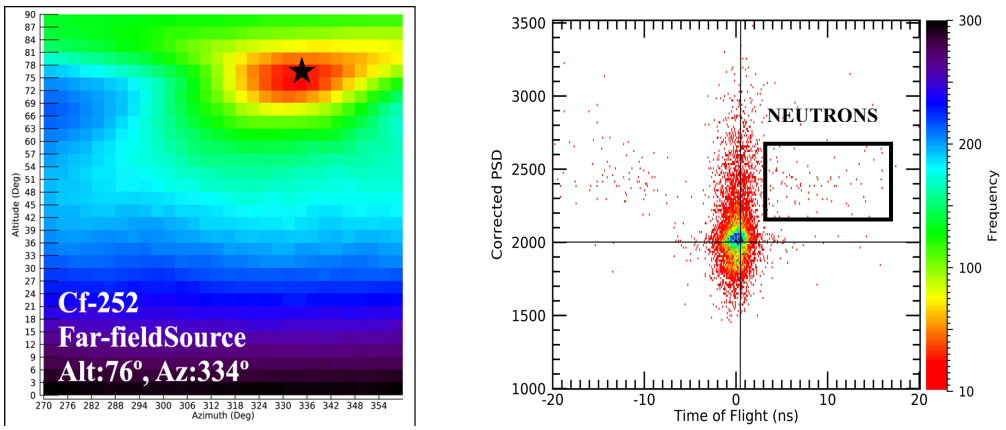

Figure 15. The source ^{252}Cf was placed far above the instrument to be considered a far-field source and the data was used to reconstruct the source image shown on the left, here the black star denotes the actual position of the source. The plot on the right from the same data set shows how PSD vs ToF distribution can be useful in separating gammas from neutrons.

5. BALOON PAYLOAD & FLIGHT

ASCOT balloon payload (Fig 16) was assembled and flown on a large scientific balloon with the help of NASA's Columbia Scientific Balloon Facility (CSBF) from Palestine, Texas. The balloon payload weighing ~1350lbs mainly consisted of the instrument, gondola, GPS compass and CSBF equipment. A flight software running on a Fitlet-H computer controlled the sending and receiving of commands, recording of the data onboard, and also interfaced to CSBF's Mini-Support Instrumentation Package (Mini SIP). A custom relay board distributed 28 V from the batteries to the instrument through filtered voltage regulators. The attitude information was provided by ADU5 GPS compass along with the pulse-per-second for timing. The instrument was held pointed at the zenith, in the center of a gondola frame and no attitude control was required.

5.1 Balloon Flight

The balloon was launched on 5th July 2018 after achieving optimum weather and wind conditions. The payload was launched at 12:10 (UTC) and it reached the float altitude of 119,000 to 123,000 feet (36.3 − 37.5 km) in two hours (Fig 17). The flight was terminated after five hours of float time and the payload was recovered close to the city of Wink (Texas) around 450 miles west of Palestine. The Crab Nebula was well within the field of view of ASCOT while at float and the instrument operated stably throughout the flight with a live time > 99% and a stable gain.

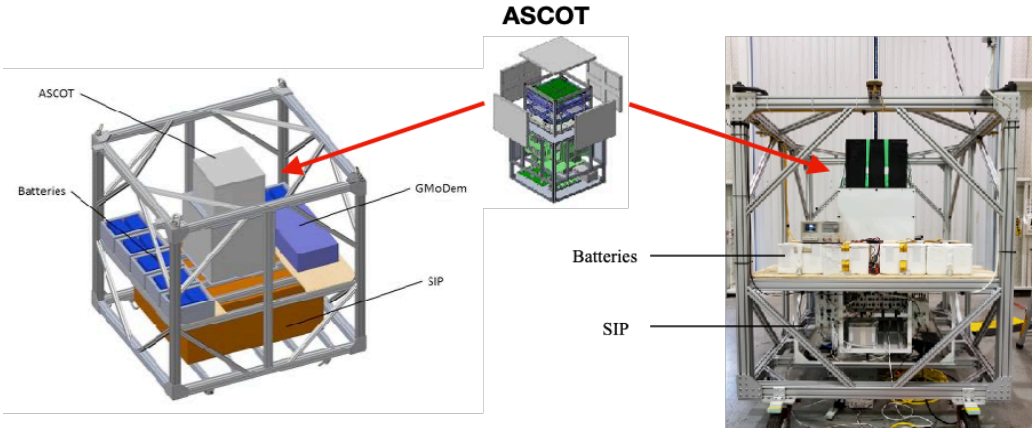

Figure 16. Mechanical drawing of ASCOT balloon payload shown (LEFT) along with the assembled payload (RIGHT) in the hangar at CSBF in Palestine, TX.

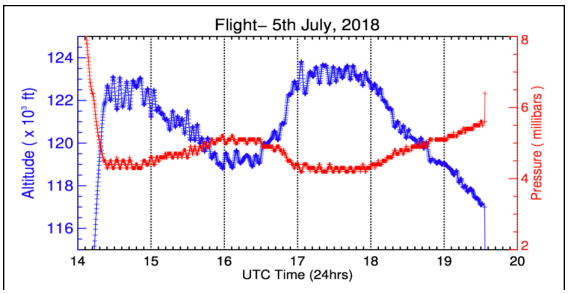

Figure 17. Altitude and Pressure shown as a function of time (UTC) during balloon float time.

5.2 Post-Flight Calibration Correction

When the energy calibrations were applied to the tagged events in the SINGLES mode (one hit either in D1 or D2) from the onboard calibration source from the flight data, it was seen that the photopeaks do not correspond to the correct energies. The reason for this was a slight change in gain of the modules between the laboratory set-up and the flight and thus the older calibration did not give accurate values for ADC to energy conversion. The photopeaks from the atmospheric 511 keV line and the onboard calibration source of ^{60}Co (lines of 1.1 MeV and 1.3 MeV) were used to correct this shift in D1 and D2 respectively. These corrected energies for a row each in a D1 module and a D2 module are shown in Fig 18.

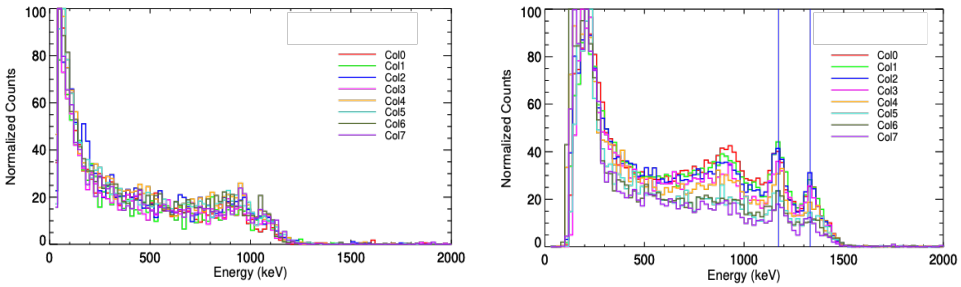

Figure 18. Plots show flight data post energy calibration correction. The events shown are from the onboard calibration source ^{60}Co aquired in the 'singles' mode. Corrected energies in the eight pixels in a single row in a D1 module (Left) and a D2 module (Right) are shown in different colors. The solid blue vertical lines show the photopeak energies of ^{60}Co at 1.1 MeV and 1.3 MeV.

Similarly, the tagged events in the coincidence mode (simultaneous hits in D1 and D2) were used to check for a shift in the ToF calibration and correct the same (Fig 19). These corrections obtained for all the possible D1- D2 pixel pairs were then applied to the 'non-tagged' events.

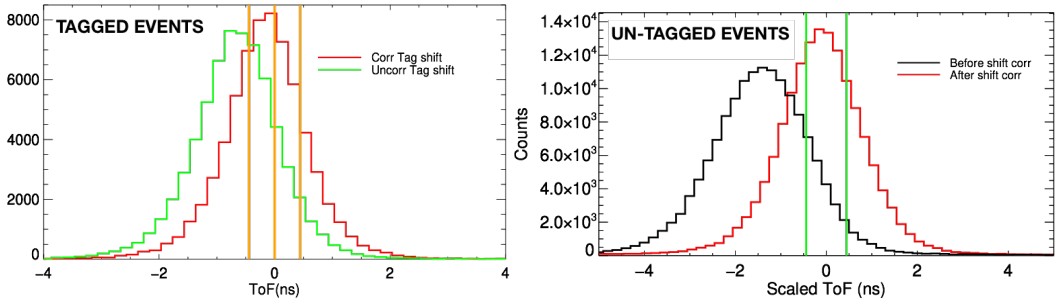

Figure 19. The tagged events in the coincidence mode (Left) were used to find the post-flight correction in the ToF calibration by finding the shift of the histogram peak from 0ns. This correction was determined for every possible pixel pair. The plot on the Right shows the same corrections applied to the non-tagged events.

6. COSMIC DIFFUSE BACKGROUND (CDG)

ASCOT was functional and observing throughout its ascent from a few feet above sea level to the floating altitude of 120,000 feet. This data is valuable in studying and analyzing the distributions of atmospheric gamma rays with altitude. An insight into the variation of gamma-rays with atmospheric depth helps in the understanding of their production and transport. The observational data was divided into three energy bands namely, 400-700 keV, 700-1500 keV and 1500-2500 keV and the differential fluxes of gamma rays were calculated to generate the growth curves[17]. The growth curves in conjunction with simulations using the ASCOT mass model were then used to estimate the CDG flux. The series of steps involved in this calculation are discussed in detail in the following sections.

6.1 Determining the count rate for the downward moving photons

The ToF distribution of the non-tagged events from the flight consists of mainly three components. One from the downward moving photons with a positive ToF shown in Green in Fig 20, a second from the upward moving photons with a negative ToF shown in Orange and a third component centered at 0 ns shown in Black arising due to the events from the activation of passive material. The ToF was calibrated and corrected along with being scaled to 0.43 ns which corresponds to a vertical separation of 13.25 cm between the two hits in D1 & D2. A PSD cut was applied in order to reject events arising from neutrons and an Earth Horizon Cut (EHC = 45°) was also applied to the data in order to omit the events arising from near the horizon. Moreover, the angle θ that the scatter vector makes zenith was restricted to being less than or equal to 25° in order to only select events with smaller scatter angles.

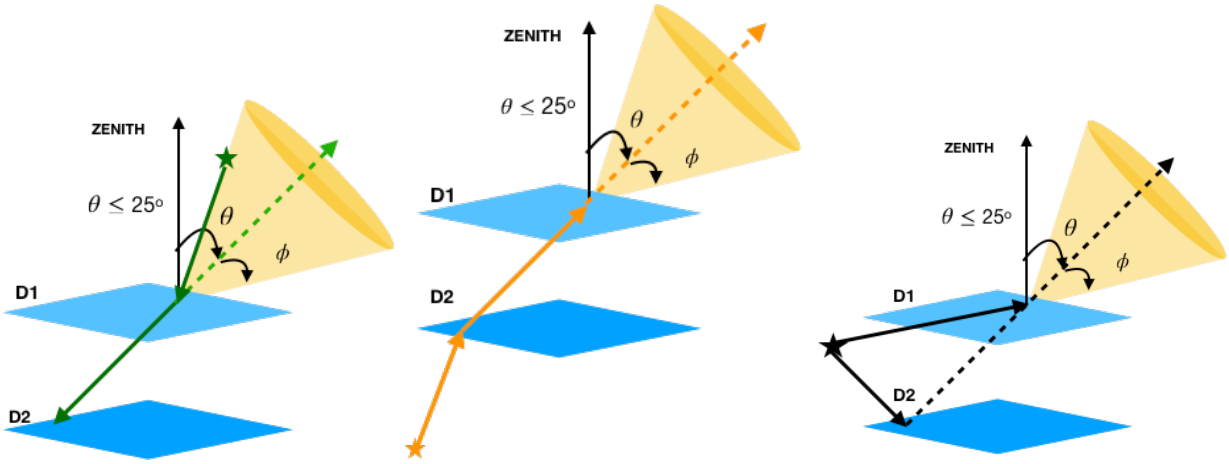

Figure 20. The drawings show an event triggering the same pixel pair but arising due to spatially different photons. The left panel shows the two hits arising from a downward moving photon (Green). The center panel shows the same pixels recording an event but from an upward moving photon. The right panel shows an event resulting from the activation of the passive material which causes near simultaneous hits and mimics an event with the same pixel pair as the other two cases. The Compton cone is shown in yellow and θ is the angle between the scatter vector and zenith.

The ToF histograms for the events in science mode and with energy in the range 0.4-0.7 MeV were plotted for different altitudes (Fig 21) and were fitted with three gaussian functions corresponding to the three components. Here the positive centroid represents the downward moving photons (shown in Green in Fig 21), the negative centroid gaussian denotes the upward moving photons (shown in Orange in Fig 21), and a third gaussian component (shown in black in Fig 21).

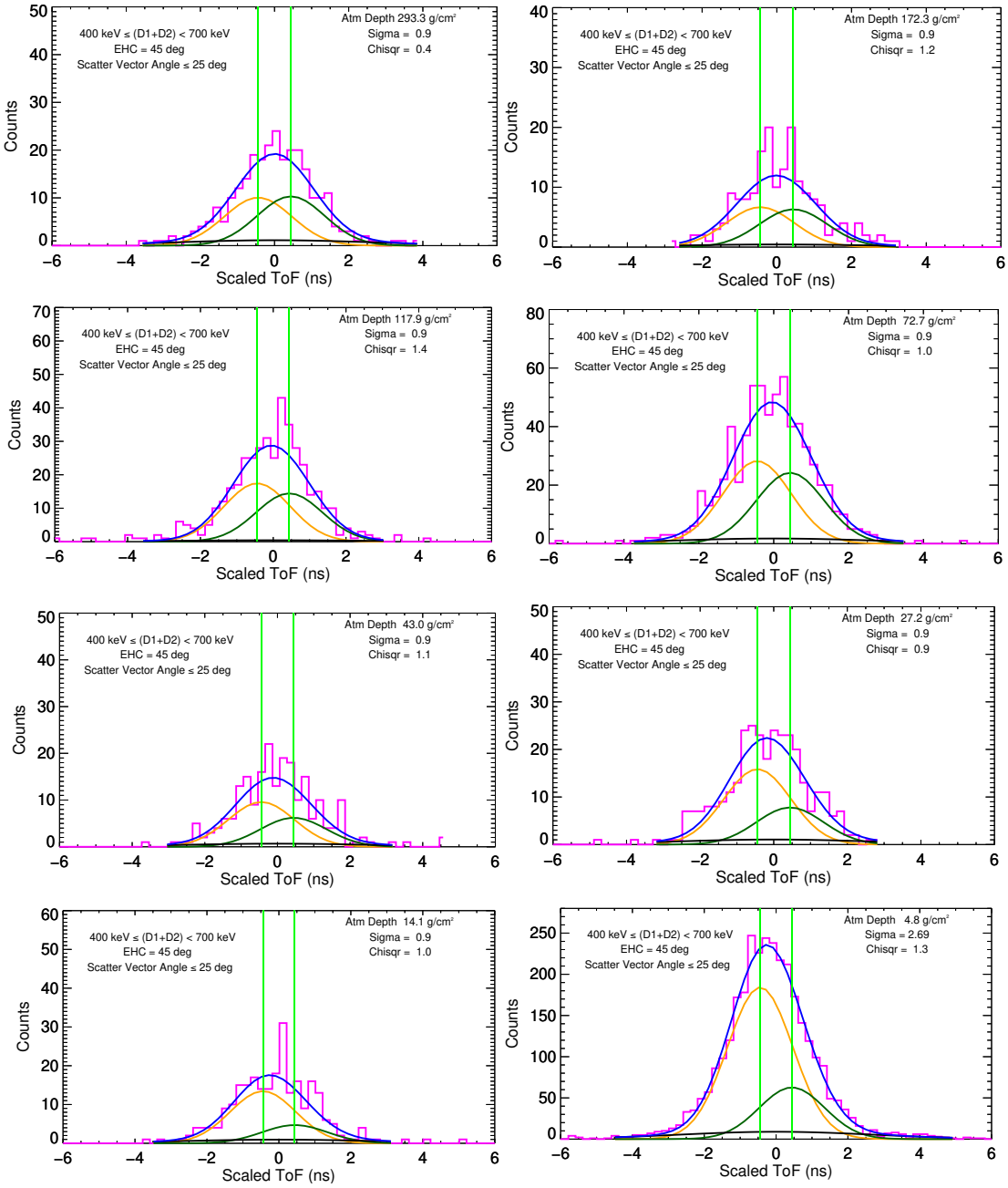

Figure 21. ToF histograms shown at various atmospheric depths, fitted with three gaussian components- downward moving photon shown in Green with a positive centroid, upward moving photons shown in Orange with negative centroid and shown in black is the component centered at 0ns. The combined fit function is shown in Blue. The data cuts applied here are - energy (400-700 keV), EHC (=45°), scatter vector angle (≤ 25°) and PSD cut.

6.2 Determining the Atmospheric Component from Growth Curve

The number of counts under the gaussian curve representing the downward moving photons and using the live time in science mode during the flight duration, the count rates were computed at different altitudes and are shown in Fig 22. The growth curve thus obtained was fitted with the following function[18] denoting the total gamma ray flux-

$$y = Ax + Be^{\frac{-x}{\tau}} \quad (1)$$

Here 'y' is the total downward gamma ray flux and 'x' is the atmospheric depth in g/cm^2. 'Ax' is the atmospheric flux component which is linear above 90 g/cm^2 of atmospheric depth, τ is the mean absorption length of gamma rays in air and is taken to be 14 g/cm^2 for this analysis and 'B' is the CDG flux. 'A' and 'B' values were determined from a best fit to the growth curve shown in blue in Fig 22.

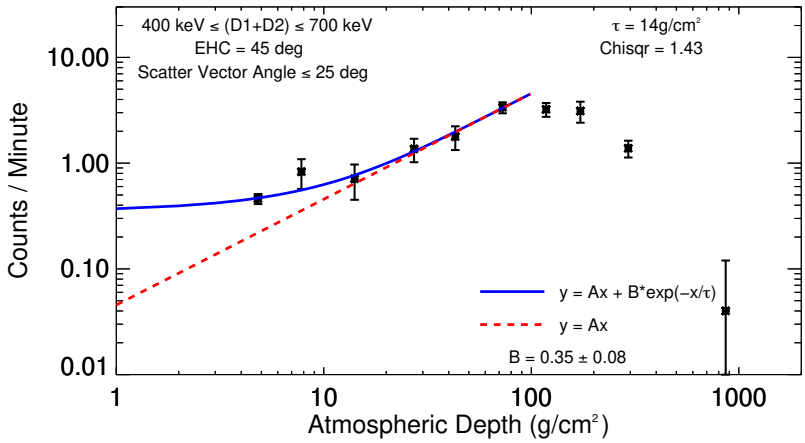

Figure 22. The growth curve for the energy range 400-700 keV is shown with solid black squares at different atmospheric depths. These points are fitted with a combination of two functions where the atmospheric component of the gamma rays is shown with the red dotted line, whereas the blue solid line represents the asymptotic value of the cosmic diffuse gamma ray background.

The errors from the gaussian fits to the ToF histograms and the flux function fit to the growth curve were added in quadrature to compute the systematic error on 'B' the observed count rate (per second) attributed to the CDG flux.

$$(CDG)_{obs} = (5.83 \pm 1.67) \times 10^{-3} \text{ counts/s} \quad (2)$$

The same steps were repeated for the other two energy ranges 700-1500 keV and 1500-2500 keV and the corresponding growth curves are shown in Fig 23. Due to the overpowering background in these ranges, only an upper limit could be obtained for the downward photon count rates at higher altitudes, which were then used for fitting the the total flux function from Eq 1.

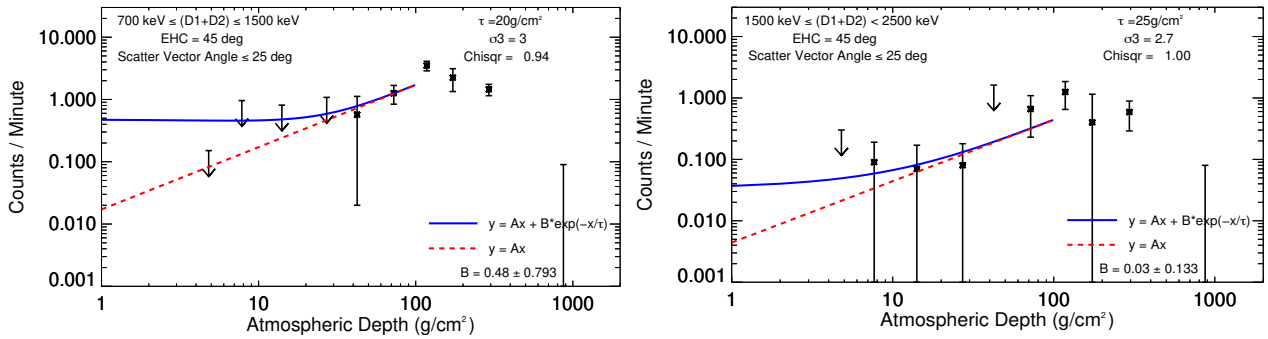

Figure 23. The growth curves for the energy ranges 700-1500 keV (Left) and 1500-2500 keV (Right) are shown with solid black squares at different atmospheric depths. These points are fitted with the function in Eq (1). The red dotted line represents the atmospheric component and the blue solid line is the extraterrestrial component of the gamma rays.

6.3 Using Simulations to estimate the Flux

MEGAlib was used to generate a mass model of ASCOT (Fig 24) along with the instrument response for a far-field power law input spectrum[19] $\propto E^{-2.1}$. The Compton events as detected by the instrument were analyzed and the same data cuts as applied to the flight data were applied to these.

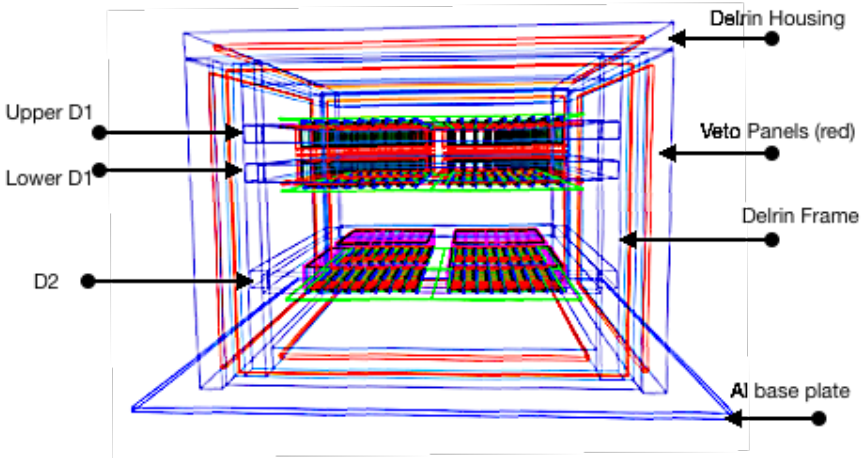

Figure 24. ASCOT mass model created using MEGAlib to generate the instrument response by simulating input energy spectra

A ratio of the photons incident on the instrument in the simulation and the count rate of the downward moving photons seen from the 'simulation' data is computed. This ratio can then be compared to the ratio for the 'observed' flight data as shown in Eq (3), and the CDG flux can be computed.

$$\frac{[\text{Sim}_{\text{ Photons Incident}}]_{0.4-0.7\text{MeV}}}{[\text{Sim}_{\text{ Counts Detected/sec}}]} = \frac{[\text{Obs}_{\text{ Photons Incident}}]_{0.4-0.7\text{MeV}}}{[\text{Obs}_{\text{ Counts Detected/sec}}]} \quad (3)$$

Substituting the input value and the resultant count rate from the simulation in Eq (3), along with the observed count rate from Eq (2), we get the following flux value-

$$[Obs_{\ Photons\ Incident}]_{0.4-0.7MeV} = (1.28 \pm 0.37) * 10^{-5} \text{ photons/cm}^2\text{/s/sr/keV} \quad (4)$$

The above steps were repeated for the energy bands 700-1500 keV and 1500-2500 keV and the flux values were computed with a 3σ upper limit.

$$[Obs_{\ Photons\ Incident}]_{0.7-1.5\ MeV} = 1.8*10^{-5} \text{ photons/cm}^2\text{/s/sr/keV} \quad (5)$$

$$[Obs_{\ Photons\ Incident}]_{1.5-2.5MeV} = 2*10^{-6} \text{ photons/cm}^2\text{/s/sr/keV} \quad (6)$$

A comparative study of these results was done with the data in the same energy range from COMPTEL[5] and the Solar Maximum Mission (SMM)[6]. And as can be seen from Fig 25 the CDG flux computed from the ASCOT flight data in all the three energy ranges agrees well with the values from the other two missions.

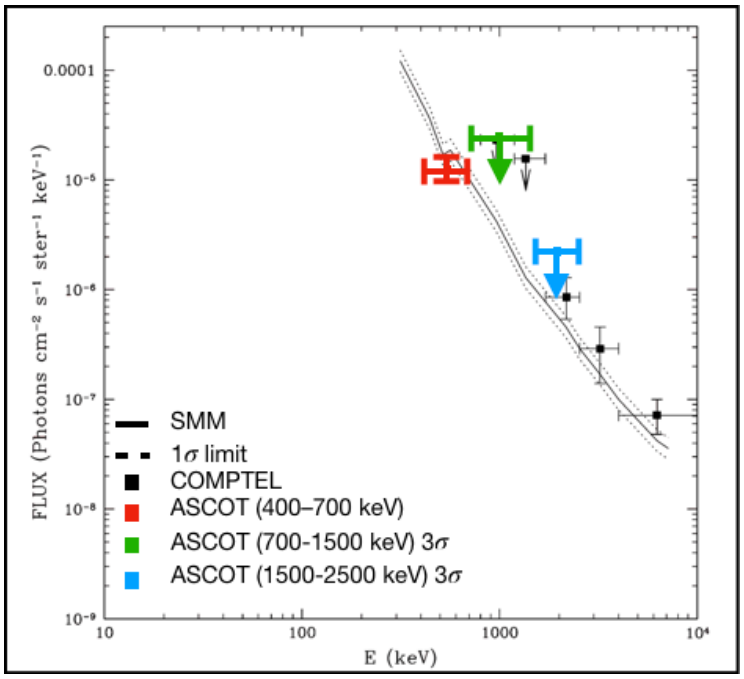

Figure 25. The CDG flux as measured by SMM is shown in solid black line along with the 1σ upper and lower limits shown by dotted lines. The COMPTEL data is shown with black squares. The three CDG flux estimates obtained from the ASCOT flight data are shown in Red, Green and Blue representing 400-700 keV, 700-1500 keV and 1500-2500 keV energy bands repectively. Figure adapted from Ref [20]).

7. FUTURE WORK

ASCOT was designed with the goal of imaging the Crab Nebula from a scientific balloon and prove the effectiveness of advanced scintillators with SiPM readouts for improving the sensitivity of medium-energy gamma-ray instrumentation. Apart from using the ascent data for the CDG flux computation, the flight data is also being analyzed to reconstruct the Crab image which involves improving and optimizing the Signal to Noise Ratio by determining the appropriate data cuts

ACKNOWLEDGEMENT

The project was supported by NASA grant NNX15AE49G.

REFERENCES

[1] Zdziarski, A. A, et al., “The canonical X-ray/gamma-ray spectrum of Seyfert 1s and low-state Galactic black hole candidates”, Astronomy and Astrophysics Supplement, v.120, p.553-558 (1996).
[2] Leising, M., Clayton, D., “The cosmic gamma-ray background from Type Ia supernovae”, Astrophys. Jour., Vol 403, 32-36 (1993).
[3] McNaron-Brown, K., et al., “OSSE observation in Blazars”, Astrophys. Jour., Vol 451 (1995).
[4] Ruiz-Lapuente, P., et al., “The origin of the cosmic gamma-ray background in the MeV range”, Astrophys. Jour., 820:142 (2016).
[5] Kappadath, S. C., et al., “The preliminary cosmic diffuse γ-ray spectrum from 800keV to 30MeV measured with COMPTEL”, Astronomy and Astrophys. Supp., Vol 120, 619-622 (1996).
[6] Watanabe, K., et al., “The MeV cosmic gamma-ray background measured with SMM”, AIP Conf. Proc., 510,471 (2000).

[7] Rodney, S. A., Riess, A. G., Strolger, L.-G., et al, The Astronomical Journal, 148, 13 (2014).
[8] Okumura, J. E., Ihara, Y., Doi, M., et al., "The Type Ia supernovae rate with Subaru/XMM-Newton Deep Survey", Pub. of the Astro Society of Japan, 66, 49 (2014).
[9] Ajello, M., Costamante, L., Sambruna, R., et al., "The evolution of SWIFT/BAT blazars and the origin of the MeV background", Astrophys Jour., 699, 603 (2009).
[10] Fishman, G. J., "Cosmic-Ray effects on diffuse gamma-ray measurements", Astrophys. Jour., 171, 163 (1972).
[11] Schönfelder, V., et al., "Instrument description and performance of the imaging gamma-ray telescope COMPTEL aboard the Compton Gamma-Ray Observatory," Astrophys. Jour. Supp. Ser., 86, 657 (1993).
[12] Bloser, P. F., et. al, "The Advanced Scintillator Compton Telescope (ASCOT) Balloon Payload" in Proc. SPIE 10699 (2018).
[13] Sharma, T., et al. "Preparations for the Advanced Scintillator Compton Telescope (ASCOT) balloon flight", Proc. SPIE 10397 (2017).
[14] Matei, C., et al., "Proton light output function and neutron efficiency of a p-terphenyl detector using a 252Cf source," Nucl. Inst. Meth. Phys. Res. A, 676, 135 (2012).
[15] Zoglauer, A., et al. "MEGAlib The Medium Energy Gamma-ray Astronomy Library", New Astronomy Reviews, Volume 50, Issue 7-8, p. 629-632 (2006).
[16] Zoglauer, A., et al., "MEGAlib: simulation and data analysis for low-to-medium-energy gamma-ray telescopes," Proc. SPIE, 7011, 70113F (2008).
[17] Ryan, J., et al., "Atmospheric Gamma Ray Angle and Energy Distributions", Journal of Geophysical Research, Vol 48, 5279-5288 (1979).
[18] Schoenfelder ,V., Lichti, G., "Energy Spectrum and evidence for extragalactic origin of diffuse gamma-radiation in the MeV range", Astrophys. Jour., 191: L1-L5 (1974).
[19] White, R. S., et al, "Cosmic Diffuse Gamma Rays from 2 to 25 MeV", Astrophys. Jour., 218:920-927 (1977).
[20] Ruiz-Lapuente, P., Korobkin, O., "Gamma-Rays from Kilonovae and the Cosmic Gamma-Ray Background", Astrophys. Jour., 892:45 (2020).